

Analyticity of the phase shift and reflectivity of electrons at a metal-semiconductor interface

D. A. Ricci,^{1,2} Y. Liu,^{1,2,*†} T. Miller,^{1,2} and T.-C. Chiang^{1,2,*‡}

¹*Department of Physics, University of Illinois at Urbana-Champaign, 1110 West Green Street, Urbana, Illinois 61801-3080, USA*

²*Frederick Seitz Materials Research Laboratory, University of Illinois at Urbana-Champaign,*

104 South Goodwin Avenue, Urbana, Illinois 61801-2902, USA

(Received 17 February 2009; published 27 May 2009)

The reflection phase shift and reflectivity as a function of electron energy at a metal-semiconductor interface are analytically related. Specifically, conjugate van Hove-type singularities are expected near a semiconductor band edge. These fundamental relations are investigated for the Pb-Si(111) interface by angle-resolved photoemission measurements of thin Pb films on Si(111) as quantum wells. A detailed determination of the reflectivity and phase shift of the Pb valence electrons across the Si valence-band edge is facilitated by using submonolayer amounts of Au as an interfaciant to systematically adjust the interface potential.

DOI: 10.1103/PhysRevB.79.195433

PACS number(s): 73.30.+y, 73.21.Fg, 79.60.Dp

Metal films are ubiquitous components of solid-state devices, and they are often conjoined with semiconductors to form metal-semiconductor interfaces. Electron reflection and transmission at such interfaces are of basic interest and play a crucial role in device functionality, especially in the quantum regime where phase coherence is a key issue. The reflectivity and reflection phase shift (and the transmission coefficient, by implication) are, however, not independent quantities; they are connected by general analytic requirements of electron propagation governed by quantum mechanics. The manifestation of these relations is best revealed by electron reflection near the band edge of a semiconductor substrate, where conjugate van Hove-type singularities as a function of electron energy are expected. The present paper is an experimental exploration and verification of this behavior. The results illustrate the intricate constraints of quantum effects on the basic electronic properties of metal-semiconductor interfaces.

The system employed in our experimental study is a set of Pb films grown on Si(111). The electrons in the Pb films, confined by the vacuum and the substrate potential, form standing waves or Fabry-Pérot interferometer modes. These modes, commonly referred to as quantum well states,¹⁻⁵ were measured by angle-resolved photoemission in our experiment. The energy positions of the quantum well states are related to the reflection phase shift at the Pb/Si interface, while the energy widths are related to the reflectivity. By varying the film thickness, the phase shift and reflectivity can be deduced at a number of discrete energies across the Si valence-band edge. These discrete energies are, however, rather sparse. This problem is overcome experimentally by adding various submonolayer amounts of Au at the Pb-Si interface for a systematic adjustment of the interface potential (Schottky barrier). Measurements from these modified interfaces yield a dense set of quantum well data suitable for verifying in detail the functional relationship of the conjugate singularities. A byproduct of this investigation is a determination of the Schottky barrier height across the Pb-Si interface as a function of the amount of the Au interfaciant, a subject matter of interest in its own right.

In our experiment, several well-ordered two-dimensional phases of Au on Si(111) were used as substrates for subsequent Pb depositions. These are the 5×2 , $\sqrt{3} \times \sqrt{3} - \alpha$, 6

$\times 6$, and $\sqrt{3} \times \sqrt{3} - \beta$ reconstructions, which are fully formed at Au coverages of $C=0.42$, 0.76, 0.96, and 0.96 monolayers (ML), respectively, in substrate units ($1 \text{ ML}=7.83 \times 10^{14} \text{ atoms/cm}^2$).⁶ In each case, the substrate was prepared by depositing Au onto a clean n -type Si(111)- (7×7) surface at room temperature and then annealing. Reflection high-energy electron-diffraction patterns were monitored to ensure single-phase coverage. The 6×6 and $\sqrt{3} \times \sqrt{3} - \beta$ reconstructions were formed at the same Au coverage but were reached through different annealing conditions following deposition, with the former resulting from a slow cool and the latter from a rapid quench. Thin Pb films were grown over the Au-terminated substrates at 60–100 K and were subsequently annealed to 100 K. For the Pb film thicknesses, one ML is defined here in terms of bulk Pb ($9.43 \times 10^{14} \text{ atoms/cm}^2$). The resulting Pb films were oriented along (111) and the film lattice constant was bulk-Pb-like and incommensurate with the Si substrate lattice. The photoemission measurements were performed at the Synchrotron Radiation Center, University of Wisconsin-Madison, using 22 eV photons, with the sample at 60–100 K. Quantum well data for Pb films grown on the Pb- $\sqrt{3} \times \sqrt{3}$ terminated Si(111) surface were adapted from a previous study to provide a reference point for $C=0 \text{ ML}$.⁷

A set of photoemission spectra at normal emission for Pb films grown on the Au- 6×6 /Si(111) surface with thicknesses ranging from 3 to 10 ML is presented in Fig. 1(a). The spectra show quantum well peaks, each of which becomes fully developed at its corresponding integer layer thickness. This discrete layer behavior facilitates a determination of the absolute film thickness by atomic-layer counting.^{8,9} Figure 1(b) displays the layer counting calibration curves, where the deposition time is correlated with the thickness in integer atomic layers that are marked by maximum intensities of the quantum well peaks. The successive peaks must be separated by 1 (or more) ML. This analysis yields a unique assignment of the film thickness for each quantum well peak.

The measured energies of the quantum well states as a function of absolute film thickness are presented in Fig. 2. Each panel corresponds to films grown over a particular Au- or Pb-terminated Si(111) surface as labeled. The energy of a given quantum well state can vary by up to $\sim 0.6 \text{ eV}$ for the

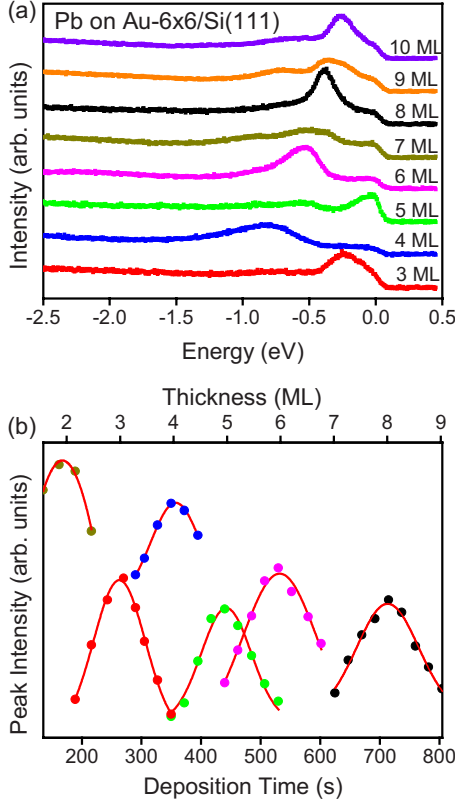


FIG. 1. (Color online) (a) Normal emission spectra from Pb films on the Au-6 \times 6/Si(111) surface. (b) Quantum well peak intensities measured as a function of Pb deposition time. The intervals between successive intensity maxima are related to monolayer increments in film thickness; this behavior permits absolute film thickness calibration.

different Au terminations, which is important for filling up the energy gaps between quantum well states. The curves and circles in the figure are derived from a fit based on the Bohr-Sommerfeld quantization rule:¹⁻⁵

$$2k(E)Nt + \phi_v(E) + \phi(E) = 2n\pi, \quad (1)$$

where $k(E)$ is the perpendicular electron wave vector, E is the electron energy, N is the number of Pb monolayers, t is the monolayer thickness, n is a quantum number, and $\phi_v(E)$ and $\phi(E)$ are the energy-dependent phase shifts at the vacuum surface and substrate interface, respectively. The bulk band dispersion $k(E)$ and the vacuum phase shift $\phi_v(E)$ are known from a first-principles calculation,¹⁰ which are employed in the present analysis. The only unknown quantity is $\phi(E)$, which can be directly extracted from Eq. (1) at the experimentally determined energies of the quantum well states.

The phase shift $\phi(E)$ is of central interest in the present work. It is part of the complex reflection coefficient at the interface, $r \exp(i\phi)$, which is given by the ratio of the reflected wave function to the incident wave function at the interface.^{11,12} Because the Hamiltonian for Bloch electrons is a smooth function of the electron wave vector k , $r \exp(i\phi)$ must be an analytic function of k . Here, we take the primary variable as the complex wave vector Δk within the Si sub-

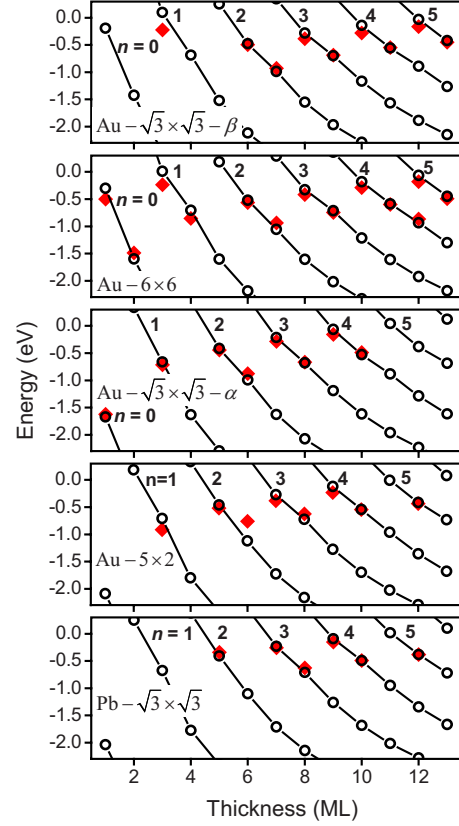


FIG. 2. (Color online) Measured (diamonds) and fitted (circles and curves) quantum well energy levels for Pb films grown on the Au- $\sqrt{3} \times \sqrt{3} - \beta$, Au-6 \times 6, Au- $\sqrt{3} \times \sqrt{3} - \alpha$, Au-5 \times 2, and Pb- $\sqrt{3} \times \sqrt{3}$ reconstructed Si(111) surfaces. The quantum number n for each state is indicated.

strate measured relative to the Si valence-band edge, which is analytically related to the wave vector within the Pb. Δk is purely imaginary within the Si gap ($E > E_0$, where E_0 is the energy of the Si valence-band edge) and real for $E < E_0$. The analyticity of $r \exp(i\phi)$ permits the following expansion to second order:

$$r \exp[i(\phi - \phi_0)] = 1 + a\Delta k + b\Delta k^2, \quad (2)$$

where ϕ_0 is the phase shift at the band edge. The leading term in the expansion is unity because the reflectivity must be unity within the Si band gap ($r=1$ for $E > E_0$). The phase shift ϕ must be a constant below the Si band edge ($\phi = \phi_0$ for $E < E_0$) based on the Huygens-Fresnel principle.¹³ These general conditions lead to strong constraints on the expansion. With Δk expressed in terms of E within the effective-mass approximation, $\Delta E \propto (\Delta k)^2$, we obtain

$$\phi = \phi_0 + a\sqrt{E - E_0}\Theta(E - E_0), \quad (3)$$

$$r = 1 - \left[a\sqrt{E_0 - E} - \frac{a^2}{2}(E_0 - E) \right] \Theta(E_0 - E), \quad (4)$$

where Θ denotes the unit step function.

Equations (3) and (4) show that both r and ϕ have a \sqrt{E} van Hove-type singularity with the same coefficient but opposite signs. These conjugate singularities, occurring on dif-

ferent sides of E_0 , are a direct result of the kinematic constraints of electron reflection near a band edge. Mathematically, they are related to the Cauchy-Riemann conditions and are unaffected by higher order terms in the expansion, which just add a smooth background. The only surviving expansion coefficient a is positive and should be on the order of

$$a \approx \frac{\pi}{\sqrt{2E_{dg}}} = 1.6 \text{ eV}^{-1/2}, \quad (5)$$

where $E_{dg} \approx 2 \text{ eV}$ is the direct gap of Si at the Brillouin-zone center. This estimate is based on extending the expansion to the midgap position of Si.

The reflectivity r is related to the quantum well peak width. The peak width is related to the decay or leakage rate of the corresponding Fabry-Pérot mode.¹⁴ A low reflectivity corresponds to a low interferometer finesse and a large peak width. Experimentally, quantum well peaks become much wider for $E < E_0$ because of a decreasing reflectivity as the Pb electrons can couple through the interface to the substrate Si states. The peak width also depends on the thickness of the film N , as a smaller N corresponds to a higher frequency of reflection loss. The relationship is given by¹⁴

$$W - W_0 = \frac{\hbar \nu}{Nt} \frac{1 - r}{\sqrt{r}}, \quad (6)$$

where W is the quantum well peak width, W_0 is the background width arising from other scattering mechanisms, and ν is the group velocity of the electrons in Pb. Here, we use an average group velocity $\hbar \nu = 12.5 \text{ eV} \cdot \text{\AA}$ determined from the bulk band structure of Pb within the energy range of interest; $W_0 = 0.07 \text{ eV}$ is taken to be the average width of all the quantum well peaks above the Si band edge.

In our analysis, the measured peak width is converted to the reflectivity r according to Eq. (6), and the phase shift ϕ is directly deduced from the peak position according to Eq. (1). The experimental results of r and ϕ for all of the different interfaces are shown in Fig. 3. The curves are the results of a global fit using Eqs. (3) and (4) with the expansion coefficient a and the band edge E_0 and phase-shift offset ϕ_0 of each interface as the fitting parameters. Because the expansion has a limited range of validity, the data are suitably truncated in the fit as seen in the figure (about 0.3 eV within the band edge). The coefficient a deduced from the fit is $1.65 \text{ eV}^{-1/2}$, which is very close to our estimate. The results presented in Fig. 3 clearly demonstrate the conjugate singularity behavior of r and ϕ . Thus, the analyticity of $r \exp(i\phi)$ is well supported by the experiment. The use of the Au interfacant in the present study allows us to fill the energy range of interest with a large number of data points, which is essential for establishing the singularity behavior in the presence of errors and noises inherent in the measurements. The circles and curves in Fig. 2 indicate the expected quantum well peak positions based on Eqs. (1) and (3) using the parameters derived from the fit.

The Si band-edge position E_0 deduced from the fit can be related to the Schottky barrier height^{15–20} for each Au-terminated interface. For the n -type Si used in the experi-

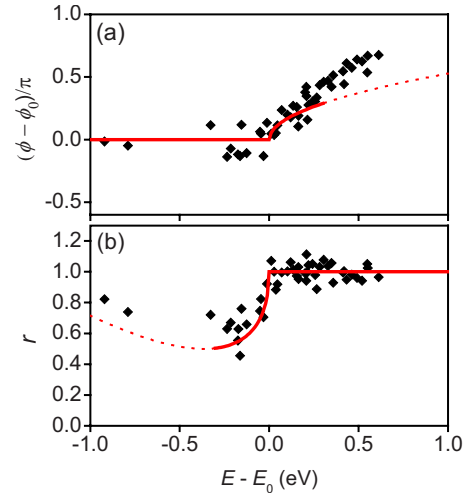


FIG. 3. (Color online) (a) Phase shift and (b) reflectivity as a function of energy. The diamonds are experimental data points. The solid curves are fits, and the dotted curves are extrapolations of the fits.

ment, the Schottky barrier height is given by $E_g - E_0$, where $E_g = 1.15 \text{ eV}$ is the absolute band gap of Si. Figure 4 shows the Schottky barrier height plotted as a function of interfacial Au coverage for the various interfaces. The approximately linear behavior suggests a simple correlation and can be well explained by an interface dipole model.²¹ Basically, the charge transfer between the metal and the semiconductor substrate across the interface creates an interface dipole, the magnitude of which depends on the electronegativities of the metal and the semiconductor involved. Since Au and Pb have significantly different electronegativities, the presence of the Au at the interface can systematically modify the interface dipole and the barrier height. This modification is expected to be a linear function of the Au coverage. The line in Fig. 4 is based on such an analysis; it depends on the known Au coverages at the interface and the electronegativities of Au, Pb, and Si, normalized in terms of the charge transfer. There are no adjustable parameters, and the line is in excellent agreement with the experimental trend.

In summary, we have performed a detailed investigation of the analytic properties of the wave-function reflection co-

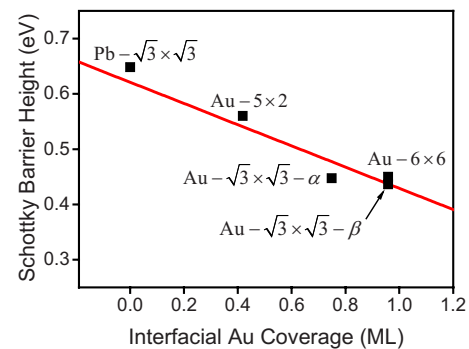


FIG. 4. (Color online) Experimental (rectangles) and predicted (line) Schottky barrier heights plotted against the interfacial Au coverage for the various Au-terminated interfaces.

efficient $r \exp(i\phi)$ at a metal-semiconductor interface (Pb-Si) for energies near the semiconductor valence-band edge. We show quite generally that the functions r and ϕ must exhibit conjugate van Hove-type singularities, one above the band edge and the other below, with the same magnitude but opposite signs. This is verified experimentally by measurements of the quantum well peak positions and widths in Pb films deposited on Si(111). An interfacial layer of Au was employed in the experiment to shift the confinement barrier, which resulted in a dense set of data over the energy range of interest. The fundamental analytic relations between the reflectivity and phase shift are of basic importance to electronic transport properties especially in the quantum or nanoscale regime where phase coherence is a key issue. A byproduct of this investigation is a detailed determination of

the Pb-Au-Si Schottky barrier height, which is well correlated with the Au concentration and the electronegativities of the elements involved. The results are consistent with an interface dipole model. The ability to tune the barrier height is important for device optimization.

This work was supported by the U.S. Department of Energy (Grant No. DE-FG02-07ER46383). We acknowledge the Petroleum Research Fund, administered by the American Chemical Society, and the U.S. National Science Foundation (Grant No. DMR-05-03323) for partial support of the personnel and the beamline facilities at the Synchrotron Radiation Center. The Synchrotron Radiation Center is supported by the U.S. National Science Foundation (Grant No. DMR-05-37588).

*Corresponding authors.

†yangliu3@illinois.edu

‡tcchiang@illinois.edu

¹T. Miller, A. Samsavar, G. E. Franklin, and T.-C. Chiang, *Phys. Rev. Lett.* **61**, 1404 (1988).

²T.-C. Chiang, *Surf. Sci. Rep.* **39**, 181 (2000).

³F. J. Himpsel, J. E. Ortega, G. J. Mankey, and R. F. Willis, *Adv. Phys.* **47**, 511 (1998).

⁴M. Milun, P. Pervan, and D. P. Woodruff, *Rep. Prog. Phys.* **65**, 99 (2002).

⁵S.-Å. Lindgren and L. Walldén, *Handbook of Surface Science*, edited by S. Holloway, N. V. Richardson, K. Horn, and M. Scheffler (Elsevier, Amsterdam, 2000), Vol. 2.

⁶T. Nagao, S. Hasegawa, K. Tsuchie, S. Ino, C. Voges, G. Klos, H. Pfnur, and M. Henzler, *Phys. Rev. B* **57**, 10100 (1998).

⁷M. H. Upton, C. M. Wei, M. Y. Chou, T. Miller, and T.-C. Chiang, *Phys. Rev. Lett.* **93**, 026802 (2004).

⁸J. J. Paggel, T. Miller, and T.-C. Chiang, *Phys. Rev. Lett.* **81**, 5632 (1998).

⁹M. H. Upton, T. Miller, and T.-C. Chiang, *Appl. Phys. Lett.* **85**, 1235 (2004).

¹⁰C. M. Wei and M. Y. Chou, *Phys. Rev. B* **66**, 233408 (2002).

¹¹P. M. Echenique and J. B. Pendry, *Prog. Surf. Sci.* **32**, 111 (1989).

¹²N. V. Smith, *Phys. Rev. B* **32**, 3549 (1985).

¹³The Huygens-Fresnel principle applies to wave propagation in general. In the present context, it states that the transmitted wave has a definitive phase relative to the incident wave, as long as the transmitted wave is propagating.

¹⁴J. J. Paggel, T. Miller, and T.-C. Chiang, *Science* **283**, 1709 (1999).

¹⁵R. T. Tung, *Mater. Sci. Eng., R.* **35**, 1 (2001).

¹⁶L. J. Brillson, *Surf. Sci.* **299-300**, 909 (1994).

¹⁷D. Cahen and A. Kahn, *Adv. Mater.* **15**, 271 (2003).

¹⁸D. R. Heslinga, H. H. Weiting, D. P. van der Werf, T. M. Klapwijk, and T. Hibma, *Phys. Rev. Lett.* **64**, 1589 (1990).

¹⁹J. H. Weaver, in *Electronic Materials: A New Era of Materials Science*, Springer Series in Solid-State Sciences, edited by J. R. Chelikowsky and A. Franciosi (Springer-Verlag, Berlin, 1991), Vol. 95, Chap. 8, p. 135.

²⁰R. F. Schmitsdorf and W. Mönch, *Eur. Phys. J. B* **7**, 457 (1999).

²¹D. A. Ricci, T. Miller, and T.-C. Chiang, *Phys. Rev. Lett.* **93**, 136801 (2004).